A 22,000-year tephrostratigraphy record of unidentified volcanic eruptions from Ternate and Tidore islands (North Maluku, Indonesia)

Audrey Faral, Franck Lavigne, Bachtiar Wahyu Mutaqin, Fatima Mokadem, Rahim Ahmad, Rohima Wahyu, Pierre Lahitte, Danang Sri Hadmoko, Estuning Tyas Mei

Version of Record: https://www.sciencedirect.com/science/article/pii/S0377027322000051
Manuscript_d0643762236de32dd163e01a8e97a624

A 22,000-year tephrostratigraphy record of unidentified volcanic eruptions from Ternate and Tidore islands (North Maluku, Indonesia)

Audrey Faral[1,2], Franck Lavigne[1,2,3], Bachtiar W. Mutaqin[4], Fatima Mokadem[2], Rahim Achmad[5], Rohima Wahyu Ningrum[5], Pierre Lahitte[6], Danang Sri Hadmoko[4], Estuning Tyas Wulan Mei[4]

[1] Université Paris 1 Panthéon-Sorbonne, 1 place du Panthéon, 75005 Paris, France
[2] Laboratoire de Géographie Physique, UMR 8591 CNRS, 1 place Aristide Briand, 92195 Meudon, France.
[3] Institut Universitaire de France, 1 rue Descartes, 75005 Paris, France.
[4] Universitas Gadjah Mada, Faculty of Geography, Bulaksumur, 55281 Yogyakarta, Indonesia.
[5] Ternate Khairun University Kampus I (UNKHAIR), Jl. Bandara Babullah, Akehuda, Ternate Utara, Kota Ternate, 97728 Maluku Utara, Indonesia
[6] UMR GEOPS, Université Paris-Saclay, CNRS, Orsay, 91405, France

Abstract

Investigating past eruptions gives a unique opportunity to understand volcanic hazards, particularly in Indonesia, where volcanic eruptions occur frequently. Here, we present the first reconstruction of the eruptive history of the Ternate and Tidore Islands (North Maluku, Indonesia) over the past 22,000 years cal. BP, based on a new identification and characterization of past volcanic events methodological approach. This multidisciplinary study (geomorphology, tephrochronology, sedimentology, geochronology, geochemistry) constitutes the first stratigraphic and chronological continuum from volcanic deposits found in a set of fifteen sections established in Ternate, Tidore, and Maitara Islands. Sedimentological and geochemical data from tephrostratigraphy studies and radiocarbon dating suggest that these islands experienced at least four major explosive events from c. 22,000 to 740 years cal. BP. The oldest event recorded is a Plinian eruption associated with a caldera-forming eruption of Telaga volcano on Tidore Island at c. 22,000 – 17,500 cal. BP. A second pumiceous eruption dated at c. 18,000 cal. BP is attributed to the last Plinian eruption of Gamalama volcano on Ternate, whose current eruptive activity is mainly strombolian or phreatomagmatic. A succession of pyroclastic deposits of phreatomagmatic origin is related to the Ngade maar formation on Ternate Island, and the abundant deposits of scoria, pumice, and ash found in all sites probably occurred c. 14,500 - 13,000 cal. BP. No eruptions of the Kie Matubu volcano on Tidore Island have been reported by human beings since their presence in the region from the 16th century, but this study highlights two late Holocene eruptions, c. 2,500 cal. BP and 740 cal. BP. This first chronostratigraphic framework from the late Pleistocene to recent eruptions in this region, sheds new light concerning the management of prediction and warning information about potential eruptions that may occur on these small volcanic islands in the future.

Keywords: eruptive history, tephrostratigraphy, caldera, radiocarbon dating, geochemistry

1. Introduction

Historical records of volcanic activity allow improving hazard assessment of volcanic islands, notably using chronostratigraphic studies. Identifying and understanding past hazards contributes to assessing the potential risk and improving the management of prediction and warning information for these vulnerable volcanic islands in the face of volcanic crises. Reconstruction of palaeoenvironmental and eruptive histories remains still fragmentary between the different Indonesian provinces. Past Indonesian eruptions are well documented in regions composed of large islands, where the population is dense, such as Java, Bali, and Lombok (e.g Rampino and Self, 1982; Self et al., 1984; Newhall et al., 2000; Fontijn et al., 2015; Vidal et al., 2015; Poliakova et al., 2017). However, little is known in regions like Sumatra or Maluku, where eruptive records are far from complete and sometimes inaccurate. To fill this gap, this study focuses on past volcanic eruptions on the small islands of Ternate and Tidore (0° 47' N, 127° 22' E; 111 km² and 116 km², respectively) in the Northern Maluku province (Fig. 1), composed of Mount Gamalama and Mount Kie Matubu (also known as Mount Tidore). Indeed, insularity and accessibility of the islands notably raise their vulnerability in particular for volcanic crisis management. Despite its remote location, Ternate is an economic hub for the Maluku region, whose population increased 5-fold between 1976 and 2017, from approximately 42,000 to 204,215 according to the last Indonesian census (Hidayat et al., 2020a). This demographic growth, which concentrated in Ternate city, led to land pressure that has resulted in the settlement of communities on the steepest slopes and closer to the summit, in areas at high risk of being affected by an eruption of Gamalama (Bacharudin et al., 1996; Méheux et al., 2007). The high density of population, services and activity make the eastern part of the Halmahera archipelago the most vulnerable to volcanic hazards (Mei et al., 2017).

This study aims to reconstruct the Ternate and Tidore islands' eruptive history and to analyze the temporal variations of eruptive style and frequency to forecast these volcanoes' potential future behavior. Since the arrival of the Portuguese and Spanish settlers in the 16th century (Taylor and Richards, 1980), only the Gamalama volcano in Ternate frequently erupted, whereas those of Tidore (i.e., Mount Kie Matubu and Mount Telaga) remained quiet. Therefore, the chronology of Gamalama's

eruptions has been inventoried for four centuries (Hidayat et al., 2020b), whereas the early-Holocene eruptive records are completely unknown for all other volcanoes of the region (Morris et al., 1983). Tephrostratigraphy is the primary approach to document the eruptive history and feed into knowledge on volcanic hazards (Martí and Folch, 2005; Groppelli and Vierreck-Goette, 2010; Marti et al., 2018; e.g for Merapi, Andreastuti et al., 2000; Newhall et al., 2000; e.g for New Zealand, Gehrels et al., 2006; Newnham et al., 1999). Here, we provide the first eruptive reconstruction of Ternate and Tidore islands over the past 22,000 years. To do so, we produced a chronostratigraphic continuum based on the accordance of (i) stratigraphic descriptions of deposits found in a set of fifteen sections (Fig. 3), (ii) whole-rock geochemical compositions of tephra samples, and (iii) ^{14}C dating of paleosols bordering the pyroclastic units.

2. Geological context

2.1. Previous research

Ternate and Tidore islands are located on Halmahera (Maluku) arc, which forms with the Sangihe (Sulawesi) arc a subduction zone of opposite position with the Maluku Sea Plate (McCaffrey et al., 1980). This process, known as double arc divergent subduction, became active in the Neogene (at c. 20 Ma for Sangihe arc and at c. 7-6 Ma for Halmahera side; Baker and Malaihollo, 1996). The Halmahera plate was thrust onto the oceanic plate and the arc consumed the oceanic lithosphere of the Maluku plate (Cardwell et al., 1980; Macpherson et al., 2003). The same process is ongoing in northeast Sulawesi at the Sangihe plate. The interaction of the Maluku Sea plate with the Halmahera plate resulted in the present volcanic arc, which moved 30 km westward and became active during the Middle Pleistocene (1 Ma) (Hall et al., 1988). The magmatic rocks of the Quaternary volcanic arc overlie ophiolitic and volcanic rocks from the succession of three back-arcs dating from the late Cretaceous, Eocene and Oligocene (Hall et al., 1991), respectively. The rocks of the present-day arc cover the eroded back-arcs and are supported by titled fault blocks in an east-dipping subduction zone (Hall et al., 1988). Therefore, the Halmahera Arc is underlain by rocks of the Neogene Arc and by the accumulation of sedimentary rocks of the adjacent basin at the back-arc region (Hall and Wilson, 2000). The modern arc of Halmahera is composed of volcaniclastic rocks (in its broadest sense)

including pyroclastic rocks, lavas and volcanic breccias. The cone-shaped stratovolcanoes (Ibu, Dukono, Gamkonora, Gamalama, Kie Matubu, Makian) of the arc have typical calc-alkaline, basaltic to andesitic magmas (Morris et al., 1983) characteristic of subduction-related magmatism intra-oceanic arc environments (Hall et al., 1988).

2.2. Study area

Ternate is composed of the active Gamalama stratovolcano (1,715 m; hereafter all elevations are given above sea level), characterized by regular activity in the form of explosive eruptions and/or degassing, interspersed with effusive eruptions producing lava flows (GVP, 2013). The record of the Gamalama eruptions is very well documented since the 16th century, from the colonial conquest of the Spice Islands by the Portuguese, then the Spanish and the Dutch. Since 1538 CE, the 77 eruptions of this volcano that have been recorded were mainly explosive, with a Strombolian and Vulcanian style (Pratomo, 2006). However, about fifteen of them were followed by lava flows, including the 1907 lava flow of Batus Angus, which reached the sea and is now a notable tourist site northeast of Ternate. The recurrence intervals of the Gamalama eruptions vary between a few months and 50 years. The eruptions are mainly characterized by the ejection of volcanic bombs and scoria, and thick clouds of ash that can be emitted for several days or even months (as during the 2015 eruption, Hidayat et al., 2020b). The eruptions occur mainly from the main central crater, however some eruptions have created secondary craters. This was the case during the explosive eruption of 1980, which formed a new crater further east of the summit crater. This latter eruption produced 10 to 15 cm of ash fall and caused the evacuation of 40,000 inhabitants of Ternate (GVP, 2013). However, it is difficult to link the many historical eruptions (of known age) to specific geological deposits, because they tend to emit similar products (basaltic andesite scoriae and/or lava flows). In addition, the formation of two maar craters on Ternate shows that there is also a high potential of phreatomagmatic eruptions at Gamalama (Fig. 2). An explosive eruption formed the 0.7×0.6 km wide Tolire maar (Fig. 2a) in 1775 CE. According to colonial and indigenous reports, the succession of base surges (GmTv unit defined by Bronto et al., 1982) killed 1,300 people, engulfing a village at the lake's current location (Bronto et al., 1982;

Setiawan et al., 2014). The eruption that led to the formation of the 0.4×0.7 km wide Ngade maar (Fig. 2b), located in the western part of Ternate city, has not yet been dated.

In the north of Tidore, the 500-m high crests and the 2.1×2.2 km wide Telaga caldera (also called Sabale) results from an undated Plinian eruption. The caldera floor is occupied by a lake and a volcanic dome, which peaks at 580 m. In the south, the Kie Matubu stratovolcano (1,730 m), also called Mount Tidore, is considered dormant by volcanologists and inactive by the local population. No eruptions have been known to occur at Tidore since at least the 16th century (Hidayat et al., 2020b).

3. Methods

3.1. Tephrostratigraphy

A systematic stratigraphic description and sampling of deposits from pyroclastic falls and Pyroclastic Density Currents (PDCs) was performed in quarries or natural outcrops-on the eastern side of Gamalama volcano, on the western coastal fringe of Maitara and Tidore island, and in a saddle between the eastern flanks of Kie Matubu and Telaga (Fig. 3). While the sections on Maitara and Tidore are island-wide, the Ternate sections are concentrated on the east and south of Gamalama. The dominant wind direction between December and May is from the northwest to the southeast, which could affect tephra deposition and completeness of the record on the south and east coast (Lessy and Abdullah, 2021). The abundance of sections (mainly from quarries) in the south-eastern part of the island is also explained by the rapid growth of Ternate city and its expansion on the slopes of the volcano. In addition, stratigraphic sections are less accessible in the northern part of the island, because it is less inhabited and largely vegetated. Each section was described according to the number of lithofacies, bed thickness, structure, grain size, type of volcanic materials (ash, scoriae, pumice, lava), color, particle shapes (angular, rounded), relative sorting, and grading pattern. Thus, this qualitative characterization of layers enables (i) to identify the type of deposit and transport mechanisms (fallout and PDCs) and (ii) to establish the relative timing of eruptive phases. Twenty-two paleosols between tephra layers and one charcoal enclosed in PDC deposits were sampled for radiocarbon dating. It was performed at Direct AMS (Washington, USA), using a NEC Pelletron 500 kV accelerator mass

spectrometer, following the preprocessing methods described in Brock et al., (2021). Paleosols underwent an acid-base-acid pretreatment to remove inorganic carbons from the sample. The remaining sample was combusted at high temperature and transformed into N_2 and CO_2 to be graphitized (Dee and Bronk Ramsey, 2000). The graphitized sample was placed in a particle accelerator, separating the ^{12}C, ^{13}C, ^{14}C ions according to their atomic mass, allowing the ^{14}C ions expressed in pMC (percent modern carbon) to be counted. The 23 radiocarbon dates, reported in BP with a 1σ confidence interval, were calibrated in cal. BP using the OxCal 4.4 online program with the IntCal 20 curve (Ramsey, 2009; Reimer et al., 2020). The mean value of radiocarbon ages (μ ± 2σ; 95.4%) is used and expressed as cal. BP in the following sections of this article (Table 2). These dates reveal the beginning of soil formation or the interruption of pedogenesis by new deposits of tephra from an eruption. Thus, the ^{14}C-dated paleosols, that are above or underlying the tephra layers, give a time interval for the eruption.

3.2. Geochemical analyses

Well-preserved deposits (pyroclastic fallout, PDCs) were sampled for whole-rock major and trace element analysis. The whole-rock samples were ultrasonically cleaned to remove all organic soil residues from tephra fragments. The samples were dried and powdered with a vibratory micro mill in agate mortar. These preparatory tasks were performed at Laboratoire de Géographie Physique (UMR 8591) in Meudon (France). The powdered samples were processed at SARM (CRPG, Nancy, France), for major elements analysis by Inductively Coupled Plasma-Atomic Emission Spectroscopy (ICP-AES) and trace elements by ICP-Mass Spectroscopy, using the methods described in Carignan et al. (2001). The sample preparation is based on a lithium borate fusion of the sample, followed by dissolution and dilution of the fusion products in HNO_3 (1 mol l-1)-H2O2 (c. 0.5% v/v)- glycerol (c. 10% v/v) mixture (Govindaraju and Mevelle, 1987). Sample solutions are analysed in a plasma excitation mass spectrometer (ICP) to quantify the elements present in the rock based on atomic wavelengths emitted (ICP-AES) or the ion mass (ICP-MS; Jarvis and Williams, 1993). Ten major elements were acquired using a Thermo Fisher ICan 6500 ICP-AES, whereas 44 trace elements were determined by a Thermo Fisher IcapQ ICP-MS (presented in Supplementary Material 2). The geochemical comparison of the 52 analysed samples allows to identify and group samples from the same volcano, or the same eruption at

best. We focussed the geochemical study mostly on immobile major, minor, and trace elements (Fe, Ti, Th, Y, Zn, Zr), which are unaffected by alteration and weathering (Chayes, 1964; Morrison, 1978; Frick and Kent, 1984). The content of immobile elements from the tephra samples provides an effective graphical method to discriminate these tephra samples and therefore determining different eruptions.

3.3. Geomorphological evolution

In order to evaluate the magnitude and volume involved during the caldera-forming eruption of Telaga, its pre-eruptive topography was modelled from the topography of the sectors still remaining using the ShapeVolc algorithm (Lahitte et al., 2012; Dibacto et al., 2020). The constraining points (CPs) were first extracted from a 30 m-resolution ASTER DEM, i.e. the DEM cells located along the ridges and planezes that represent the least eroded surfaces (Lavigne et al., 2013; Germa et al., 2015). Then, the volcanic shape before the caldera-forming eruption was modelled by setting up the parameters that define the surface of revolution best adjusted to the CPs. Parameters to be fitted were: the summit location (Xc, Yc); the elevation (Zc); the parameters defining the shape of the generatrix (i.e. the curve rotating around the center); the distortion parameters (azimuth of the long-axis and eccentricity) that account for the ellipticity (i.e. the not perfectly circular shape) of the volcano. In addition, the uneroded surfaces of the current landscape (planezes, ridges, uppermost interfluves remaining after erosion) were reconstructed, as well as a model of summit-collapse scarp evolution. This allows to compare the pre-eruptive surface with a model of the erosional evolution to establish the new post-caldera surface. Finally, we computed the volume balance between modelled surfaces (i.e. each eruptive or erosion stage), to estimate the volume lost between the pre-eruptive surface and the floor of the caldera in order to define the size of the eruption (Lahitte et al., 2012; Lavigne et al., 2013).

4. Results

4.1. Stratigraphy and geochronology

Our stratigraphic analysis consists of twenty-four stratigraphic logs, fifteen of which are presented in Figure 3. Deposits are composed of alternating layers of tephra and paleosols. The three schematic logs, TL-CP5, KM-8, and TN-CP12, displayed in Figure 4, represent the different types of deposits found in all sites. The lithological naming (e.g. a, b, c in Fig. 3 and Fig. 4) of the sections is

independent for each log, i.e., the same unit can be labelled with different letters according to its stratigraphic position. Paleosols, tephra fallout, and PDC units were correlated between the sections wherever possible using stratigraphy, geochronology, and geochemistry. The radiocarbon ages (Fig. 3) are consistent with the stratigraphy and the deposits were emplaced during the late Pleistocene and the middle Holocene (Fig. 3, Table 2).

4.1.1. Pyroclastic fall deposits

Dark grayish scoria-fall deposits and ballistic bombs are found on 7 out of the 15 sections presented in Figure 3. The thickest scoria fall deposit (>2 m) is located south and east of Ternate (TN-CP6-j and TN-CP18-b-c-d; Fig. 3), 4 km from the summit of Mount Gamalama, and consists, as in all other sections, of a dark moderately sorted scoriaceous lapilli breccia, with juvenile lithic fragments interbedded with fine and coarse ash and ballistic bombs and blocks up to 10 cm. No alteration horizon or paleosols interrupt the pyroclastic fallout that is 3 to 5 m thick on Ternate and Maitara. Paleosols underlying massive succession of 2 to 6 meters of scoria fall deposits on Tidore, Ternate, and Maitara (TL-CP1, TL-CP5, TN-CP6, and MATCP4 in Fig. 3) are dated around 14,500 - 13,000 cal. BP (Table 2).

Pumice-fall deposits in nine sections suggest sub-Plinian or Plinian eruptions in the region. We can observe two groups of pumice fallout based on their white and gray color. The base of 4 sections located on Ternate (TN-CP10-b, TN-CP17-a, TN-CP6-a in Fig. 3) and Maitara (MAT-CP1-b in Fig. 3, Supplementary Material 1) displays a 1 to 6 meters thick unit composed of well-sorted, slightly rounded white pumiceous lapilli and blocks (<10 cm), highly vesicular and glass-rich. On top of these white pumices and separated by successive paleosols, we note the presence of several units of rounded, well-sorted grayish pumiceous lapilli (TN-CP10, TN-CP17, TL-CP5, TL-CP1, TN-CP6, TL-CP16/17, MAT-CP1/4 in Fig. 3). The widely dispersed 10 to 40 cm thick grayish fallout deposits could come from other Plinian-style (but possibly smaller magnitude) eruptions of the numerous volcanoes in the area (Mount Telaga, Gamalama, Kie Matubu, Dukono, Ibu, Gamkonora, Makian in Fig. 1).

4.1.2. *Pyroclastic density current deposits*

All six sections north-northeast of Tidore (Fig. 3) are composed at their base of stratified deposits of light-coloured, rounded, normally graded pumiceous lapilli breccia with blocks up to 10 cm (TL-CP5-b in Fig. 4). These deposits are mostly composed of glass-rich, highly vesicular pumice lapilli and do not contain a large quantity of lithic fragments (less than 10%). The wavy bedded with low angle cross-stratification in between, with reversely graded subunits in the TL-CP sections (Fig. 4 and Fig. 5a) indicate that the pumice deposits are composed of several dilute PDC units (surges). The dating of four paleosols underlying these dilute PDC deposits on Tidore (TL-section in Fig. 3) reveals synchronous dates (Table 2): 22,433 ± 103 cal. BP, 21,646 ± 180 cal. BP, 22,239 ± 99 cal. BP, 21,918 ± 128 cal. BP, respectively. A new paleosol was formed above the dilute PDCs (pumiceous surge layers) at about 17, 500 years cal. BP ago (over TL-CP1-3, Fig. 3).

South of Tidore Island, on the western flank of Kie Matubu, section KM-1 is composed of ash matrix in which pumice and dense juvenile fragments are mixed. The gray pumiceous lapilli and blocks (10-15 cm in diameter) are angular, moderately vesicular and glass-rich clasts. The dense to poorly vesicular andesite fragment, highly crystalline and clast size up to angular blocks (> 60 cm), are the most abundant component on KM-1 section. The KM-1 located at about 100 m and confined to a small river valley is 8 m thick of dense PDCs and distinctly normally graded. The age of the KM-1 deposit is provided by charcoal enclosed in a dense PDC deposit west of Kie Matubu (KM-1 in Fig. 3) and dated to 2669 ± 77 cal. BP (Table 2).

On the southeastern flanks of Kie Matubu, located at about 300 m, five sections (KM-3-4-5-6-8) up to 3 to 8 m thick deposits are composed of two units. At the base of these sections, the most prominent deposits consist of an ash matrix mixed with unsorted dense andesite lapilli and blocks fragments, size up to 1 meter in diameter, non-vesicular, angular and crystal-rich (Fig. 3, KM-8 in Fig. 4, Table 1). These monolithological deposits with normal grading indicate that this juvenile component, dominated by dense fragments, are dense PDCs (block-and-ash flow type). Dense PDC deposits of KM-3-4-5-6-8 are distinguished from KM-1 deposits by the absence of vesicular pumiceous clasts.

Dilute PDC (ash-cloud surge type) deposits are observed at the top of the dense PDC deposits (Fig. 3 and KM-8-a in Fig. 4). The lithofacies of these new units are very different to the one on which they rest (Table 1). Dilute PDC deposits, between 40 cm and 1 m thick, are composed of a matrix of coarse beige-yellowish ash mixed with gray, dense juvenile non-vesicular lapilli and blocks (>20 cm) that are similar to the underlying dense PDC deposits (Fig. 3, KM-8-b in Fig. 4, Table 1). Formed 90 cm above these dilute-PDC deposits (ash-cloud surge type), the most recent paleosol of our study (KM-8-1) is dated at 740 ± 26 cal. BP (Table 2).

On Ternate, on the southeast flank of Gamalama, we were able to identify a second type of dilute PDC deposits. The TN-CP12 section, located at about 70 m in altitude, is composed of plane-parallel or diffuse wavy-parallel stratified units with a repetition of thin beds composed of coarse, gray ash interbedded with fine juvenile lithic lapilli fragments (>3 cm) (TN-CP12-a in Fig. 4 and Fig. 5b). This massive deposit is located c. 1000 m east of the crater, in the mid-distal zone from the vent and at least 4 meters thick (we could not reach its base). We interpret these deposits as base surge deposits, not only based on their lithological and sedimentological characteristics but also by their location (Cas and Wright, 1987). Indeed, the TN-CP12 section is located about ten meters west of the tuff ring crater of the Ngade Maar (65 m).

4.2. Geochemical and textural correlation of tephra

4.2.1. Major and minor elements

Among the units described previously, 52 geochemical analyses were carried out and are presented in Supplementary Material 2. The K_2O-SiO_2 diagram (Fig. 6a) shows that eruptions belong to the calc-alkaline volcanic series, typical of island volcanic arcs. The geochemical analysis samples span a range from basaltic-andesite to dacite, although four samples display a more mafic composition (Fig. 6a).

The comparison of major, minor and trace element contents allows to identify and group the deposits of the same volcano or same eruption. Discrimination of seven geochemical groups (Fig. 6 and Fig. 7) is based on *(i)* geochemically similar composition; *(ii)* correlation of stratigraphic position of

samples from the same group; *(iii)* description of the deposit of the hypothetical group and; *(iv)* location of the deposit relative to the assumed volcanic source.

In order to differentiate the collected tephras, Fe_2O3- and K_2O contents are plotted against TiO_2-
275 contents - the three oxide concentrations being affected by magmatic differentiation. However, TiO_2 is stable during weathering, leaching and metamorphism process of altered igneous rocks deposits (Fig. 6; Floyd and Winchester, 1978; Frick and Kent, 1984). From this diagram, several clearly defined groups of samples are identified and nominated with capital letters. The first two defined clusters, called Group A and Group B, contain five and seven samples, respectively. These specimens represent a dacitic
280 cluster and the andesitic compositions in the K_2O-SiO_2 diagram (Fig. 6a). Group A corresponds to plurimetric white pumice fallout and flow deposits at the base of several logs from Ternate, Tidore, and Maitara (Fig. 3). However, group B's grayish pumice fallout differs geochemically from Group A by its Fe_2O_3 and K_2O contents. The three samples of Group C correspond to basaltic specimens in the K_2O-SiO_2 diagram (Fig.6a). They are sufficiently different from a total population of samples to warrant
285 being placed in a singular group. Group D includes seven samples of grayish pumice fallout (Fig. 6b). As can be seen in figure 6b, about 30 samples do not fall in any of these groups and are too scattered to be aggregated in a single group. This suggests that they were generated by other eruptions. Harker diagrams with SiO_2 on the X-axis and all major and minor elements on the Y-axis are presented in Supplementary Material 2. The first three groups clearly highlighted in Figure 6 with TiO_2 on the X-
290 axis, are not as well differentiated from the rest of the samples in these diagrams, which are even less discriminating for the remaining 30 samples (see Supplementary Material 2).

4.2.2. Trace elements

Oxide content (Fe_2O-K_2O) used in figure 6 vary due to their sensitivity to weathering effects. Therefore, the abundance of minor and trace immobile elements in volcanic rocks, particularly Ti, Zr, Y, Nb
295 and Th, are used in this study to discriminate products of a subalkaline magma series of each eruption. Immobile element contents remain the same since the formation of the rock. These elements time-invariant contents represent a unique "fingerprint" of an eruption (e.g Chayes, 1964; Morrison, 1978; Frick and Kent, 1984; Hastie et al., 2007; Portnyagin et al., 2020). Immobile trace element plots are the most discriminating

diagrams and allow distinguishing samples that may have similar major and minor geochemical element contents.

Four immobile trace elements are plotted against TiO_2 in the Harker-type variation diagram. The four first groups defined in figure 6 are clearly separated for all immobile trace elements in figure 7. Moreover, using these diagrams, most other samples (white symbol in Fig. 6) can now be clustered in three other geochemical groups. Nine grayish andesitic rock samples ranked in Group E were found only on Tidore. Five of them were sampled from the Kie Matubu flanks (KM- sample, Fig. 7). The sixth group of thirteen samples, retrieved from mixed ash and scoria falls, is identified as Group F. Being constituted of six well-sorted and rounded gray pumice samples, Group G clearly refers to the andesitic series in figure 6a. This group consists of similar grayish pumice fall deposits like those found in groups B and D. However, it is well separated from them due to its higher TiO_2 content. According to the geological map of Ternate, the basaltic-andesite "Gam 1907" sample was collected on a lava flow called Batu Angus, which was formed during the 1907 effusive eruption of Gamalama (Bronto et al., 1982). The major element contents of "Gam 1907" are similar to the C, F, and G groups. Thus, samples of these groups are likely to have been generated by Gamalama. The stratigraphic survey and the magmatic evolution of the trace element content between C, F, and G groups and Gam 1907 suggest they represent several pre-1907 Gamalama eruptions, as further discussed in section 5.5.

5. Discussion

The correlation between the stratigraphic position of the tephra samples, the geochronological constraints of radiocarbon dating, and the geochemical groups are used to provide the first chronology of the eruptive events that took place on the islands of Ternate and Tidore before the 16th century.

5.1. *Caldera-forming eruption of Telaga (between 22,000 and 17,500 cal. BP)*

Based on the coherence of the radiocarbon ages of the underlying and overlying paleosols and the geochemical homogeneity of the dacitic rocks of group A, the oldest volcanic event presented in this study is a Plinian eruption of the Telaga volcano, which occurred between 22,000 and 17,500 cal. BP. This eruption produced thick pumiceous dilute PDCs within the caldera (4 to 10 m thick, Fig. 3), as well as to the north of the edifice (Fig. 8b and c). The dilute PDCs with pumiceous lapilli size

fragments are found at Tidore and Maitara up to 4 km from Telaga volcano (Fig. 8a). Simultaneously or consecutively to the dilute PDCs generated during the collapse of the eruptive column, well-sorted millimeter to centimeter-sized pumice fallout spread out in the distal zone, up to the north of Ternate, with a deposit thickness of at least 1 meter (Fig. 8a). The northwestwardly progressive decrease in thickness of the pumice deposits from north Tidore to Ternate (Fig. 8a) validates the hypothesis of these deposits originating from Telaga volcano instead of Kie Matubu.

Despite the absence of lithic-rich PDC deposits on Telaga's slopes, we argue that this Plinian eruption between 22,000 to 17,500 cal. BP may have formed the present caldera, which is a typical feature of caldera-forming eruptions. Indeed, the caldera rim is located at only 4 km from the sea, suggesting that lithic-rich PDCs may be underwater today. At the time of the eruption, the sea level was about 100 to 115 meters below the present one, leaving a single island connecting Ternate, Maitara, Tidore, and Halmahera (Sathiamurthy and Voris, 2006). Therefore, the dilute PDCs spread as far as northwest Maitara and Ternate Island through the current strait, which was emerged at that time.

Based on a numerical reconstruction model of the Telaga cone before the eruption, the volcano peaked at c. 1,210 m (Fig. 9). The height difference between the pre-eruptive and basal caldera surface elevations (e.g. 900 meters at the paleosummit level) resulted in a calculated volume of removed material of 1.20 km^3 ± 0.28 km^3 (2σ uncertainty, 95% confidence interval).

5.2. *Later eruptions of Telaga (c. 16,500 cal. BP)*

Geochemical groups B and D, composed of slightly altered gray pumice fallout, may be linked to more recent Telaga volcano eruptions. These andesitic rocks are geochemically close to those of the Plinian caldera-forming eruption (group A, Fig. 6a). We conclude that one or more fallout deposits resulting from one or two sub-Plinian-style eruptions of the Telaga occurred after 16,595 ± 127 cal. BP (Fig. 3 and Table 2). However, it is only a hypothesis that should be corroborated by additional mineralogical and petrological analyses of samples.

5.3. *Plinian eruption of Gamalama (c. 18,000 - 16,000 cal. BP)*

Group G is represented by well-sorted deposits that are composed of angular gray pumice lapilli fallout with clast size of 3-8 cm in diameter and which is identified in three sections on Ternate (TN-CP6-3, TN-CP10-2, TN-CP17-1 Fig. 3). It sits is in the same stratigraphic position as group B, i.e., above the paleosol overlying the pumice-fall deposits of the caldera-forming eruption. Even if the stratigraphic position and descriptions found to be the same between the B and G groups, these significant geochemical discrepancies allow discriminating two volcanoes at the origin of these deposits. The lapilli (>3 cm) and pumiceous blocks (c. 8-10 cm) found in deposits of thicknesses between 70 cm and 1.3 m on Ternate suggests that the source of the volcano is close by and cannot come from one of the volcanoes of the Halmahera arc. The nearest volcanoes of Ternate and Tidore islands are located at distance of fifty kilometers (Makian, Jailolo) and more than a hundred kilometers (Gamkonora and Todoko, Fig.1). One of their eruptions could not have deposited such large pumice at Ternate, even downwind. We conclude that pumice fallout deposits from group G might be the result from a sub-Plinian eruption of Gamalama, based on the fragment size and deposit thickness at least 2 km from the volcano summit. Paleosols below and above the pumice fallout from a likely Gamalama eruption yield a ^{14}C age interval between 18,217 ± 143 cal. BP and 16,178 ± 99 cal. BP (Table 2). Nevertheless, to validate this hypothesis it would be necessary to have access to the distal downwind deposits of this eruption on Halmahera island, in order to compare the stratigraphic descriptions and the geochemistry to group G deposits.

5.4. *Vulcanian or strombolian eruptions of Gamalama*

The massive deposit over 2 to 5 meters thick at the top of sections MAT-CP4- (i), MAT-CP1-(d-i), TL-CP1-(h), TN-CP6- (j) (Fig. 3; TN-CP13, MAT-CP2, MAT-CP3 in Supplementary Material 1), composed of ash fallout, scoriaceous lapilli, juvenile lithic fragments (size up to 2 cm), blocks and ballistic (up to 10 cm) projections, are overlying paleosols dated around 14,500 - 13,000 cal. BP. This might be a Gamalama eruption releasing large volumes in a short period, or several successive phases of the same eruption, which would have lasted several months (e.g., the 9-month eruption of Galunggung in 1982 in Java, Gerbe et al., 1991), leaving no time for pedogenesis to develop. These

continuous deposits may suggest a Strombolian or Vulcanian eruption, similar to recent Gamalama eruptions of VEI 1-2 known since the 16th century (Hidayat et al. 2020b).

5.5. *Ngade Maar formation caused by phreato-magmatic eruption (c. 14,500 - 13,000 cal. BP)*

The samples of group F, composed of bedded and laminated successions of fine pyroclastic deposits with ash and scoriae, are found in 5 sections and particularly over several meters thick around the Ngade maar in Ternate (TN-CP6, TL-CP5, TL-CP1, Fig. 3, Supplementary Material 1). This geochemical group F is also composed of dilute PDC (base surge) samples from Ternate's TN-CP12 section. The decreasing thickness of these stratified tuff ring deposits from Ternate towards Maitara and Tidore attests that they were emplaced during a phreatomagmatic eruption that formed the Ngade maar (Cas and Wright, 1991; Scharf et al., 2001). The interaction between magma and water during the eruption explains the high fragmentation of the juvenile fragments found in the base surge deposit of the TN-CP12 section.

Furthermore, the basaltic to andesite composition of Gamalama magmas, represented by the lava sample from the 1907 CE eruption or by the samples of its last Plinian eruption (group G), is comparable to the composition of the phreatomagmatic deposits surrounding the maar (Fig. 6 and Fig. 7). From the paleosols beneath the phreatomagmatic deposits, the Ngade maar can be dated approximately after 14,500 - 13,000 cal. BP (TN-CP1, TN-CP5, MAT-CP1 in Table 2, Fig. 3). The eruption would have started with explosive interactions between magma and water. This interaction triggered dilute PDCs (base surges), whose ash and gas clouds spread out very quickly, expanding radially and reaching several kilometers from the source. TN-CP12 (Fig. 5b), about 1 km east of the crater, displays soft, wavy parallel-bedded facies because these base surge deposits are in the distal zone (>900 m) of the event. Low angle cross bedding typically found in base surges will be located closer to the source in the proximal zone (c. 200 m) (Vazquez and Ort, 2006). Then, ballistic projections composed of lithic lapilli fragments, sometimes forming bomb sags in the eruptive base are superimposed to form thick fallout. The deposits of the crater of the Ngade maar are incomplete (TN-CP11, TN-CP12, TN-CP13), reworked and partially missing owing to constructions and quarries linked

to the progressive extension of the urbanization of Ternate around the maar, limiting the stratigraphic study.

5.6. *Late Holocene eruptions of Kie Matubu (c. 2,669 cal. BP and c. 740 cal. BP)*

While the eruptive history of Kie Matubu in Tidore remained totally unknown so far, we identified at least two eruptions of this volcano during the late Holocene. On the western flank of Kie Matubu, at 150 m elevation, the KM-1 section is constituted of a coarse massive dense PDC with dense juvenile blocks and normal grading (Fig. 3 and 4; see 4.1.2 Results section). This highlights a first basaltic to andesitic eruption of Kie Matubu (group E, Fig. 6), that is constrained to 2,669 ± 77 cal. BP (Table 2, Fig. 3), based on the radiocarbon-dated of a charcoal enclosed in the dense PDCs of KM-1. These pumice and ash flows may have resulted from Vulcanian-type (or Plinian-type) fountain or eruption column collapses (as observed during the Soufrière Hills eruption on Montserrat: Cole et al., 2002; Druitt et al., 2002). The high concentration of pumice-and-ash PDC deposits channelled in topographic pathways (like the KM-1 section) were likely formed by segregation from collapsing fountains, which spread away from the event at inferred velocities of c. 10 $m.s^{-1}$ (Cole et al., 2002).

On the south-eastern flank of Kie Matubu at 350 m, the KM-3-4-5-6-8 stratigraphic sequences, 3 km from the summit, display unsorted and massive multimetric block-and-ash flows deposits (Fig. 3 and 4; see 4.1.2 Result section), which are overlain by less than 1 m of dilute PDCs (Fig. 3, Supplementary Material 1). The lower part of the paleosol formed above the dilute PDC deposits in the KM-8 section, on the east flank of Kie Matubu, yields a ^{14}C age of 740 ± 26 cal. BP (c. 1210 cal. CE) (Table 2, Fig. 3). However, finding a charcoal within the deposit would help to better refine the age of the eruption. Thus, the calculated age of 740 ± 26 cal. BP (c. 1210 cal. CE) might be slightly younger than the actual age of the deposits, i.e. the dense PDCs may be older than the 13th century. According to the stratigraphic sequences and age of the overlying paleosol, this eruptive sequence in KM-3-4-5-6-8 suggests a second eruption of Kie Matubu prior to the 13th century caused by dome collapse (Branney & Kokelaar, 2003; e.g Charbonnier and Gertisser, 2011; Gertisser et al., 2012). Block-and-ash flow deposits are typically associated with steep-sided andesitic volcanic cones during a collapse of the volcanic dome (e.g for Montserrat : Cole et al., 2002; for Colima : Reyes-Dávila et al., 2016).

Caused by gravitational collapse or explosion of the lava dome, block-and-ash flows can extend up to 10 km or at high velocities (range from 5 to 20 m s^{-1}, the front occasionally up to 60 m s^{-1}) and are controlled by gravity and usually valley-confined (Gertisser et al., 2011; Cole et al., 2002). The PDCs found in the south-eastern sections are constituted by two phases. Near the ground, a dense current composed mostly of blocks mixed with ash flows down the slopes at high speed. Above the dense PDC, a turbulent ash cloud spreads out, and settles over a thickness of about 1 m. The geochemical similarity of major and trace elements in the KM- sample (Group E) between the western and eastern Kie Matubu deposits set may suggest a single eruption of this volcano. However, unlike the KM-1 section to the west of the volcano, there is no pumice component in the eastern flank sections (KM-3-4-5-6-8). In addition, the two radiocarbon ages, one dated from a charcoal in the dense PDC (KM-1, west) and the second from a paleosol formed above the ash cloud surge (KM-8, east), are outside the 2-sigma range of the calibrated ^{14}C ages. Therefore, the two types of dense PDCs from the western flank and the eastern flank should be interpreted as separate events.

5.7 Reconsidering volcanic hazard and risk in north Maluku

The late Holocene volcanic activity from Kie Matubu reconstructed here suggests an unconsidered volcanic risk at Tidore Island. Indeed, this volcano was so far perceived by residents and authorities as inactive, compared to the nearby Gamalama active volcano. The Ternate authorities have a detailed Gamalama volcanic hazard map (Bacharudin et al., 1996), a prevention, and an emergency evacuation plan based on an eruptive scenario of VEI>2 (Marfai et al., 2019). This volcanic risk management is a result of the knowledge of the recent eruptive history of Gamalama since 16th century. On the other hand, although the BPBD (National Disaster Management Agency) has an office based in Tidore, Kie Matubu volcano is not subject to any particular monitoring to this day. This lack of monitoring and of a specific eruption management plan for the Tidore volcanoes is explained by the unrecorded eruptive history of Kie Matubu and Telaga volcanoes. Our study reveals two recent eruptions of Kie Matubu, the latest soon before the 13th century. However, this record is still largely incomplete. The volcanic unrest of El Chichón volcano in 2000 or Sinabung volcano in 2010 after respectively 500 and 400 years of quiescence led to the evacuation of thousands of people and the death

of 2000 people in the case of the Mexican volcano exemplifies the need to study the geological history of volcanoes considered as dormant (Espíndola et al., 2000; Hendrasto et al., 2012). This potential new volcanic activity would not necessarily cause an unprecedented disaster but would have a great impact on the population and economy of the North Maluku region.

The recent "Sister Island" program based on the “Sister village” concept (Cho et al., 2016; Mei et al., 2019, 2018) foresees maritime evacuation of the Ternate inhabitants towards Tidore if Gamalama were to erupt (Mei et al., 2019; Hidayat et al., 2020a, 2020b). At present, there in no contingency plan in place to evacuate the population of Tidore to Ternate and neighboring islands in the case of an eruption of Telaga or Kie Matubu. Governmental and other agencies concentrate their volcanic disaster risk reduction activities on the 127 volcanoes recognized as being active in this archipelagic country, and especially on the 77 type A volcanoes, which are those with an active eruptive history after 1600 (77 volcanoes; Pratomo, 2006). Type B volcanoes are those volcanoes having history of eruptions before 1600 (29 volcanoes); and type C volcanoes are those having no historical record of eruptions, but still show traces of volcanic activity, such as solfatara or fumaroles (Pratomo, 2006). Telaga or Kie Matubu are not listed in the third category due to the absence of volcanic activity. It is important to mention that more than 80% of the known eruptions identified in Indonesia occurred since 1900, which indicates the need to study the geological record of these volcanoes (Siebert et al., 2010). In other words, knowledge of the geological history by stratigraphic techniques is insufficient and we must keep in mind that the historical record is still very limited for most volcanoes. This is no exception for the volcanoes of the Maluku region. If in this work we are interested in the volcanoes of Ternate and Tidore, the geological and historical record of the active volcanoes of the region (Amasing, Bibinoi, Dukono, Gamkonora, Ibu, Jailolo, Makian, Tigalalu, Tobaru, Todoko-Ranu - Global Volcanism Program) is unknown.

Conclusions

Based on sedimentary records and tephrostratigraphy, we document in this study the first recent geologic eruptive history of the Ternate and Tidore islands since c. 22,000 cal. BP, which have been excluded from volcanological studies so far, and for which no local narrative records are available.

Telaga's volcanic activity in Tidore has been characterized by at least two Plinian or sub-plinian eruptions: a caldera-forming eruption between 22,000 and 17,500 cal. BP. and a second eruption which occurred c. 16,500 cal. BP. These pyroclastic deposits reveal that Telaga had a lower eruption frequency since the late Pleistocene, with possible inactivity period during the Holocene. New data from Gamalama at Ternate reveal that the eruptive style of the volcano has evolved since the late Pleistocene, suggesting at least one subplinian eruption between 18,000 - 16,000 cal. BP and a phreatomagmatic eruption on the southern flank that resulted in the formation of the Ngade maar during the Pleistocene-Holocene transition. Although no eruptive history of Kie Matubu at Tidore has been recorded to date, the Holocene stratigraphic record reveals the occurrence of two andesitic eruptions: a first fountain-column collapse eruption 2600 years ago and more recently, a lava-dome collapse eruption before the 13th century. The eruptive records proposed in this study are still largely incomplete, due to the complexity and abundance of deposits from the different volcanoes in the region. Knowledge of the eruptive history aims to contribute to volcanic hazard assessment. This first geological record from the late Pleistocene to the Holocene provides insight into the scale of occurrence of the eruption risk at Ternate and Tidore Islands. This partial geological record that highlights Tidore's volcanic activity might raise the issue of incorporating the risk of dormant volcanoes into volcanic monitoring and initiate an appropriate management plan at Tidore, despite the fact that in human memory, the activity of the Kie Matubu and Telaga volcanoes has never threatened the population.

Acknowledgments

This research has been carried out in the frame of the Master degree of A. Faral at the University Paris 1 Pantheon-Sorbonne (Master DYNARISK). The field trip in 2020 was funded by the Institut Universitaire de France (IUF, a research project of Prof. F. Lavigne, which focuses on the eruptive history of poorly studied volcanoes in Indonesia). The authors are thankful to the Laboratory of Physical Geography (Theme Volcanography), who supported and funded the geochemical analysis and radiocarbon dating. We also thank the Universitas Gadjah Mada (UGM, Yogyakarta) and the Universitas Khairun (UNKHAIR) for local support of their experts. Special thanks to « L'association

Européenne de Volcanologie » (L.A.V.E) for its financial contribution to A. Faral's thesis. Finally, this research is a contribution to the Work Package "Environmental and Societal Dynamics of Risks" of the Cluster of Excellence "Territorial and Spatial Dynamics" (LabEx DynamiTe). We thank the two reviewers, Ralf Gertisser and Karen Fontijn, for their in-depth reviews of this paper.

References

Andreastuti, S., Agency, G., Alloway, B. V, Ernest, I., and Smith, M. (2000). A detailed tephrostratigraphic framework at Merapi Volcano , Central Java , Indonesia : Implications for eruption predictions and hazard assessment. *J. Volcanol. Geotherm. Res.* 100(4), 51–67. doi:10.1016/S0377-0273(00)00133-5.

Bacharudin, R., Martono, A., and Djuhara, A. (1996). Disater prone zone map of Gamalama volcano, Ternate, Maluku Utara, Scale 1 : 25 000. *Bandung Volcanol. Surv. Indones.*

Baker, S., & Malaihollo, J. (1996). Dating of Neogene igneous rocks in the Halmahera region: arc initiation and development. *Geological Society, London, Special Publications*, 106(1), 499–509.

Branney, M. J., and B. P. Kokelaar (2002), Pyroclastic Density Currents and the Sedimentation of Ignimbrites, *Geol. Soc. Mem.,* vol. 27, Geol. Soc., London.

Brock, F., Higham, T., Ditchfield, P., and Bronk Ramsey, C. (2021). Current pretreatment methods for AMS radiocarbon dating at the Oxford Radiocarbon Accelerator Unit (ORAU). *Radircarbon* 52(1), 103–112. doi:10.1017/S0033822200045069.

Bronto, S., Hadisantono, R. ., and Lockwood, J. . (1982). *Peta geologi Gunungapi Gamalama, Ternate, Maluku Utara*. , ed. D. Vulkanologi [Bandung Indonesial]: Direktorat Vulkanologi Available at: https://www.worldcat.org/title/peta-geologi-gunungapi-gamalama-ternate-maluku-utara-geologic-map-of-gamalama-volcano-ternate-north-maluku/oclc/13633331 [Accessed April 21, 2019].

Cardwell, R. K., Isacks, B. L., and Karig, D. E. (1980). The spatial distribution of earthquakes, focal mechanism solutions, and subducted lithosphere in the Philippine and northeastern Indonesian Islands. *Tecton. Geol. Evol. Southeast Asian seas islands* 23, 1–35. doi:10.1029/gm023p0001.

Carignan, J., Hild, P., Mevelle, G., Morel, J., and Yeghicheyan, D. (2001). Routine analyses of trace elements in geological samples using flow injection and low pressure on-line liquid chromatography coupled to ICP-MS: A study of geochemical reference materials BR, DR-N, UB-N, AN-G and GH. *Geostand. Newsl.* 25(2-3), 187–198. doi:10.1111/j.1751-908x.2001.tb00595.x.

Cas, R. A., and Wright, J. V. (1991). Subaqueous pyroclastic flows and ignimbrites: an assessment.

Bull. Volcanol. 53(5), 357–380. doi:10.1007/BF00280227.

Cas, R., and Wright, J. (1987). *Volcanic successions: Modern and Ancient: A geological approach to processes, products and successions*. Springer S. 528 p doi:10.1007/978-0-412-44640-5.

Charbonnier, S. J., and Gertisser, R. (2011). Deposit architecture and dynamics of the 2006 block-and-ash flows of Merapi Volcano, Java, Indonesia. *Sedimentology* 58(6), 1573–1612. doi:10.1111/j.1365-3091.2011.01226.x.

Chayes, F. (1964). A petrographic distinction between Cenozoic volcanics in and around the open oceans. *J. Geophys. Res.* 69(8), 1573–1588. doi:10.1029/JZ069i008p01573.

Cho, S. E., Won, S., and Kim, S. (2016). Living in harmony with disaster: Exploring volcanic hazard vulnerability in Indonesia. *Sustain.* 8(9), 848. doi:10.3390/su8090848.

Cole, P. D., Calder, E. S., Sparks, R. S. J., Clarke, A. B., Druitt, T. H., Young, S. R., et al. (2002). Deposits from dome-collapse and fountain-collapse pyroclastic flows at Soufrière Hills Volcano, Montserrat. *Geol. Soc. Mem.* 21(1), 231–262. doi:10.1144/GSL.MEM.2002.021.01.11.

Dee, M., and Bronk Ramsey, C. (2000). Refinement of graphite target production at ORAU. *Nucl. Instruments Methods Phys. Res. Sect. B Beam Interact. with Mater. Atoms* 172(1-4), 449–453. doi:10.1016/S0168-583X(00)00337-2.

Dibacto, S., Lahitte, P., Karátson, D., Hencz, M., Szakács, A., Biró, T., et al. (2020). Growth and erosion rates of the East Carpathians volcanoes constrained by numerical models: Tectonic and climatic implications. *Geomorphology* 368, 107352. doi:10.1016/j.geomorph.2020.107352.

Druitt, T. H., Young, S. R., Baptie, B., Bonadonna, C., Calder, E. ., Clarke, A. ., et al. (2002). Episodes of cyclic Vulcanian explosive activity with fountain collapse at Soufriere Hills Volcano, Montserrat. *Geol. Soc. London Mem.* 21, 281–306. doi:10.1144/GSL.MEM.2002.021.01.13.

Espíndola, J. M., Macías, J. L., Tilling, R. I., & Sheridan, M. F. (2000). Volcanic history of El Chichón Volcano (Chiapas, Mexico) during the Holocene, and its impact on human activity. Bulletin of Volcanology, 62(2), 90–104. https://doi.org/10.1007/S004459900064

Floyd, P. A., and Winchester, J. A. (1978). Identification and discrimination of altered and metaphorphosed volcanic rocks using immobile elements. *Chem. Geol.* 21(3-4), 291–306.

Fontijn, K., Costa, F., Sutawidjaja, I., Newhall, C. G., and Herrin, J. S. (2015). A 5000-year record of multiple highly explosive mafic eruptions from Gunung Agung (Bali, Indonesia): implications for eruption frequency and volcanic hazards. *Bull. Volcanol.* 77(7), 1–15. doi:10.1007/s00445-015-0943-x.

Frick, C., and Kent, L. E. (1984). Drift pumice in the Indian and South Atlantic Oceans. *South African J. Geol.* 87(1), 19–33.

Gehrels, M. J., Lowe, D. J., Hazell, Z. J., and Newnham, R. M. (2006). A continuous 5300-yr Holocene cryptotephrostratigraphic record from northern New Zealand and implications for tephrochronology and volcanic hazard assessment. *Holocene* 16(2), 173–187. doi:10.1191/0959683606hl918rp.

Germa, A., Lahitte, P., and Quidelleur, X. (2015). Construction and destruction of Mont Pelée volcano: Volumes and rates constrained from a geomorphological model of evolution. *J. Geophys. Res. Earth Surf.* 120(7), 1206–1226. doi:10.1002/2014JF003355.

Gertisser, R., Cassidy, N. J., Charbonnier, S. J., Nuzzo, L., and Preece, K. (2012). Overbank block-and-ash flow deposits and the impact of valley-derived, unconfined flows on populated areas at Merapi volcano, Java, Indonesia. *Nat. Hazards* 60(2), 623–648. doi:10.1007/s11069-011-0044-x.

Gertisser, R., Charbonnier, S. J., Troll, V. R., Keller, J., Preece, K., Chadwick, J. P., et al. (2011). Merapi (Java, Indonesia): Anatomy of a killer volcano. *Geol. Today* 27(2), 57–62. doi:10.1111/j.1365-2451.2011.00786.x.

Govindaraju, K., and Mevelle, G. (1987). Fully automated dissolution and separation methods for inductively coupled plasma atomic emission spectrometry rock analysis. application to the determination of rare earth elements: Plenary lecture. *J. Anal. At. Spectrom.* 2(6), 615–621. doi:10.1039/JA9870200615.

Global Volcanism Program, 2013. Gamalama (268060) in Volcanoes of the World, v. 4.10.1 (29 Jun 2021). Venzke, E (ed.). Smithsonian Institution. Downloaded 13 Jul 2021 (https://volcano.si.edu/volcano.cfm?vn=268060). doi.org/10.5479/si.GVP.VOTW4-2013

Groppelli, G., and Viereck-Goette, L., eds., Stratigraphy and Geology of Volcanic Areas: Geological Society of America Special Paper 464, Boulder, Colorado, USA (293 pp)

Hall, R., Audley-Charles, M. G., Banner, F. T., Hidayat, S., and Tobing, S. L. (1988). Late Palaeogene-Quaternary geology of Halmahera, eastern Indonesia: initiation of a volcanic island arc. *J. - Geol. Soc.* 145(4), 577–590. doi:10.1144/gsjgs.145.4.0577.

Hall, R., Nichols, G., Ballantyne, P., Charlton, T., and Ali, J. (1991). The character and significance of basement rocks of the southern Molucca Sea region. *J. Southeast Asian Earth Sci.* 6(3-4), 249–258. doi:10.1016/0743-9547(91)90071-5.

Hall, R., and Wilson, M. E. J. (2000). Neogene sutures in eastern Indonesia. *J. Asian Earth Sci.* 18(6),

781–808. doi:10.1016/S1367-9120(00)00040-7.

Hastie, A. R., Kerr, A. C., Pearce, J. A., & Mitchell, S. F. (2007). Classification of altered volcanic island arc rocks using immobile trace elements: Development of the Th-Co discrimination diagram. *Journal of Petrology*, 48(12), 2341–2357. https://doi.org/10.1093/PETROLOGY/EGM062

Hendrasto, M., Surono, Budianto, A., Kristianto, Triastuty, H., Haerani, N., et al. (2012). Evaluation of volcanic activity at sinabung volcano, after more than 400 years of quiet. *J. Disaster Res.* 7(1), 37–47. doi:10.20965/jdr.2012.p0037.

Hidayat, A., Marfai, M. A., and Hadmoko, D. S. (2020a). Eruption hazard and challenges of volcanic crisis management on a small Island: A case study on Ternate Island - Indonesia. *Int. J. Geomate* 18(66), 171–178. doi:10.21660/2020.66.ICGeo43.

Hidayat, A., Marfai, M. A., and Hadmoko, D. S. (2020b). The 2015 eruption of Gamalama volcano (Ternate Island–Indonesia): precursor, crisis management, and community response. *GeoJournal*, 1–20. doi:10.1007/s10708-020-10237-w.

Jarvis, K.E., Williams, J.G., 1993. Laser ablation inductively coupled plasma mass spectrometry (LA-ICP-MS): a rapid technique for the direct, quantitative determination of major, trace and rare-earth elements in geological samples. *Chem. Geol*. 106, 251-262. https://doi.org/10.1016/0009-2541(93)90030-M

Lahitte, P., Samper, A., and Quidelleur, X. (2012). DEM-based reconstruction of southern Basse-Terre volcanoes (Guadeloupe archipelago, FWI): Contribution to the Lesser Antilles Arc construction rates and magma production. *Geomorphology* 136(1), 148–164. doi:10.1016/j.geomorph.2011.04.008.

Lavigne, F., Degeai, J.-P., Komorowski, J.-C., Guillet, S., Robert, V., Lahitte, P., et al. (2013). Source of the great A.D. 1257 mystery eruption unveiled, Samalas volcano, Rinjani Volcanic Complex, Indonesia. *Proc. Natl. Acad. Sci.* 110(42), 16742–16747. doi:10.1073/pnas.1307520110.

Lessy, M. ., and Abdullah, R. (2021). Forecasting of Significant Wave Height and Period at Western Waters of Ternate Island, North Maluku. *Techno J. Penelit.* 10(1).

Macpherson, C. G., Forde, E. J., Hall, R., and Thirlwall, M. F. (2003). Geochemical evolution of magmatism in an arc-arc collision: The Halmahera and Sangihe arcs, eastern Indonesia. *Geol. Soc. Spec. Publ.* 219(1), 207–220. doi:10.1144/GSL.SP.2003.219.01.10.

Marfai, M. A., Mei, E. T. W., and Retnowati, A. (2019). *Pengurangan Risiko Bencana Gunungapi*

Gamalama Ternate. , ed. B. Jl. Grafika No. 1 Yogyakarta: Gadjah Mada University Press.

Martí, J., Groppelli, G., & Brum da Silveira, A. (2018). Volcanic stratigraphy: A review. *Journal of Volcanology and Geothermal Research*, 357, 68–91. doi.org/10.1016/J.JVOLGEORES.2018.04.006

Marti, J., Folch, A., 2005. Anticipating volcanic eruption. In: Marti, J., Gerald, G.J.E. (Eds.), Volcanoes and the Environment. Cambridge University Press, Cambridge, United Kingdom.

McCaffrey, R., Silver, E. A., and Raitt, R. W. (1980). 'Crustal structure of the Molucca Sea collision zone, Indonesia.', in *The tectonic and geologic evolution of Southeast Asian seas and islands.* (Washington, DC : AGU), 161–177. doi:10.1029/gm023p0161.

Méheux, K., Dominey-Howes, D., and Lloyd, K. (2007). Natural hazard impacts in small island developing states: A review of current knowledge and future research needs. *Nat. Hazards* 40(2), 429–446. doi:10.1007/s11069-006-9001-5.

Mei, E. T. ., Putri, R. F., Sadali, M. I., Febrita, D., Yulandari, E. D., Anggriani, M., et al. (2019). Sister School for Merapi Volcano Disaster Risk Reduction. *IOP Conf. Ser. Earth Environ. Sci.* 256(1). doi:10.1088/1755-1315/256/1/012022.

Mei, E. T. W., Fajarwati, A., Sudibyo, J., Sari, I. M., Safitri, D., Rusmayanti, F., et al. (2018). *Sister Village: Strategi Alternatif Mitigasi Bencana Gunungapi*. Yogyakarta: Gadjah Mada University Press.

Mei, E. T. W., Meilyana Sari, I., Fajarwati, A., and Safitri, D. (2017). Assessing the Social Economic and Physical Vulnerabilities to Gamalama Volcano. *Education*, 1–36. doi:10.2991/icge-16.2017.7.

Morris, J. D., Jezek, P. A., Hart, S. R., and Gill, J. B. (1983). 'The Halmahera Island arc, Molucca Sea collision zone, Indonesia: a geochemical survey.', in *The tectonic and geologic evolution of Southeast Asian seas and islands.* (Washington, DC : AGU), 373–387. doi:10.1029/gm027p0373.

Morrison, M. A. (1978). The use of 'immobile' trace elements to distinguish the palaeotectonic affinities of metabasalts: applications to the Paleocene basalts of Mull and Skye, Northwest Scotland. *Earth Planet. Sci. Lett.* 39(3), 407–416. doi:10.1016/0012-821X(78)90029-8.

Newhall, C. G., Bronto, S., Alloway, B., Banks, N. G., Bahar, I., Del Marmol, M. A., et al. (2000). 10,000 Years of explosive eruptions of Merapi Volcano, Central Java: Archaeological and modern implications. *J. Volcanol. Geotherm. Res.* 100(1-4), 9–50. doi:10.1016/S0377-0273(00)00132-3.

Newnham, R. M., Lowe, D. J., and Alloway, B. V. (1999). Volcanic hazards in Auckland, New Zealand: a preliminary assessment of the threat posed by central North Island silicic volcanism based on the

Quaternary tephrostratigraphical record. *Geol. Soc. Spec. Publ.* 161(1), 27–45. doi:10.1144/GSL.SP.1999.161.01.04.

Poliakova, A., Zonneveld, K. A. F., Herbeck, L. S., Jennerjahn, T. C., Permana, H., Kwiatkowski, C., et al. (2017). High-resolution multi-proxy reconstruction of environmental changes in coastal waters of the Java Sea, Indonesia, during the late Holocene. *Palynology* 41(3), 297–310. doi:10.1080/01916122.2016.1162865.

Portnyagin, M.V., Ponomareva, V.V., Zelenin, E.A., Bazanova, L.I., Pevzner, M.M., Plechova,A.A., Rogozin, A.N., Garbe-Schönberg, Di, 2020. TephraKam: Geochemical database ofglass compositions in tephra and welded tuffs from the Kamchatka volcanic arc(northwestern Pacific). *Earth Syst. Sci. Data* 12, 469–486.https://doi.org/10.5194/essd-12-469-2020.

Pratomo, I. (2006). Klasifikasi gunung api aktif Indonesia, studi kasus dari beberapa letusan gunung api dalam sejarah. *Indones. J. Geosci.* 1(4), 209–227. doi:10.17014/ijog.vol1no4.20065.

Rampino, M. R., and Self, S. (1982). Historic eruptions of Tambora (1815), Krakatau (1883), and Agung (1963), their stratospheric aerosols, and climatic impact. *Quat. Res.* 18(2), 127–143. doi:10.1016/0033-5894(82)90065-5.

Ramsey, C. B. (2009). Bayesian analysis of radiocarbon dates. *Radiocarbon* 51(1), 337–360. doi:10.1017/s0033822200033865.

Reimer, P. J., Austin, W. E. N., Bard, E., Bayliss, A., Blackwell, P. G., Bronk Ramsey, C., et al. (2020). The IntCal20 Northern Hemisphere Radiocarbon Age Calibration Curve (0-55 cal kBP). *Radiocarbon* 62(4), 725–757. doi:10.1017/RDC.2020.41.

Reyes-Dávila, G. A., Arámbula-Mendoza, R., Espinasa-Pereña, R., Pankhurst, M. J., Navarro-Ochoa, C., Savov, I., Vargas-Bracamontes, D. M., Cortés-Cortés, A., Gutiérrez-Martínez, C., Valdés-González, C., Domínguez-Reyes, T., González-Amezcua, M., Martínez-Fierros, A., Ramírez-Vázquez, C. A., Cárdenas-González, L., Castañeda-Bastida, E., Vázquez Espinoza de los Monteros, D. M., Nieto-Torres, A., Campion, R., … Lee, P. D. (2016). Volcán de Colima dome collapse of July, 2015 and associated pyroclastic density currents. Journal of Volcanology and Geothermal Research, 320, 100–106. https://doi.org/10.1016/J.JVOLGEORES.2016.04.015

Sathiamurthy, E., and Voris, K. H. (2006). Maps of Holocene Sea Level Transgression and Submerged Lakes on the Sunda Shelf. *Nat. Hist. J. Chulalongkorn Univ. Suppl.* 2, 1–44.

Scharf, by B., Pimrng, M., Boehrer, B., Büchel, G., Friese, K., Kusel-Fetzmatrí, E., et al. (2001). Limnogeological studies of maar lake Ranu Klindungan, East Java, Indonesia. *Amaz. Limnol. Oecologia Reg. Syst. Fluminis Amaz.* 3(3-4), 487–516.

Self, S., Rampino, M. R., Newton, M. S., and Wolff, J. A. (1984). Volcanological study of the great Tambora eruption of 1815. *Geology* 12(11), 659–663. doi:10.1130/0091-7613(1984)12<659:VSOTGT>2.0.CO;2.

Setiawan, F., Wibowo, H., Santoso, A. B., Nomosatryo, S., and Yuniarti, I. (2014). Karakteristik danau asal vulkanik; Studi kasus Danau Tolire, Pulau Ternate. *Limnotek-Perairan Darat Trop. di Indones.* 21(2), 103–114.

Siebert, L., Simkin, T., and Kimberly, P. (2010). *Volcanoes of the World*. Third edit. Univ. of California Press.

Sparks, R. S. J. (1986). The dimensions and dynamics of volcanic eruption columns. *Bull. Volcanol.* 48(1), 3–15.

Taylor, P. M., and Richards, M. N. (1980). *F.S.A De Clercq's - Ternate : The Residency and its Sultanate. Translated from Dutch.* Washington, D.C: Smithsonian Institution Libraries Edition.

Vazquez, J. A., and Ort, M. H. (2006). Facies variation of eruption units produced by the passage of single pyroclastic surge currents, Hopi Buttes volcanic field, USA. *J. Volcanol. Geotherm. Res.* 154(3-4), 222–236. doi:10.1016/j.jvolgeores.2006.01.003.

Vidal, C. M., Komorowski, J. C., Métrich, N., Pratomo, I., Kartadinata, N., Prambada, O., et al. (2015). Dynamics of the major plinian eruption of Samalas in 1257 A.D. (Lombok, Indonesia). *Bull. Volcanol.* 77(9), 1–24. doi:10.1007/s00445-015-0960-9.

Figures

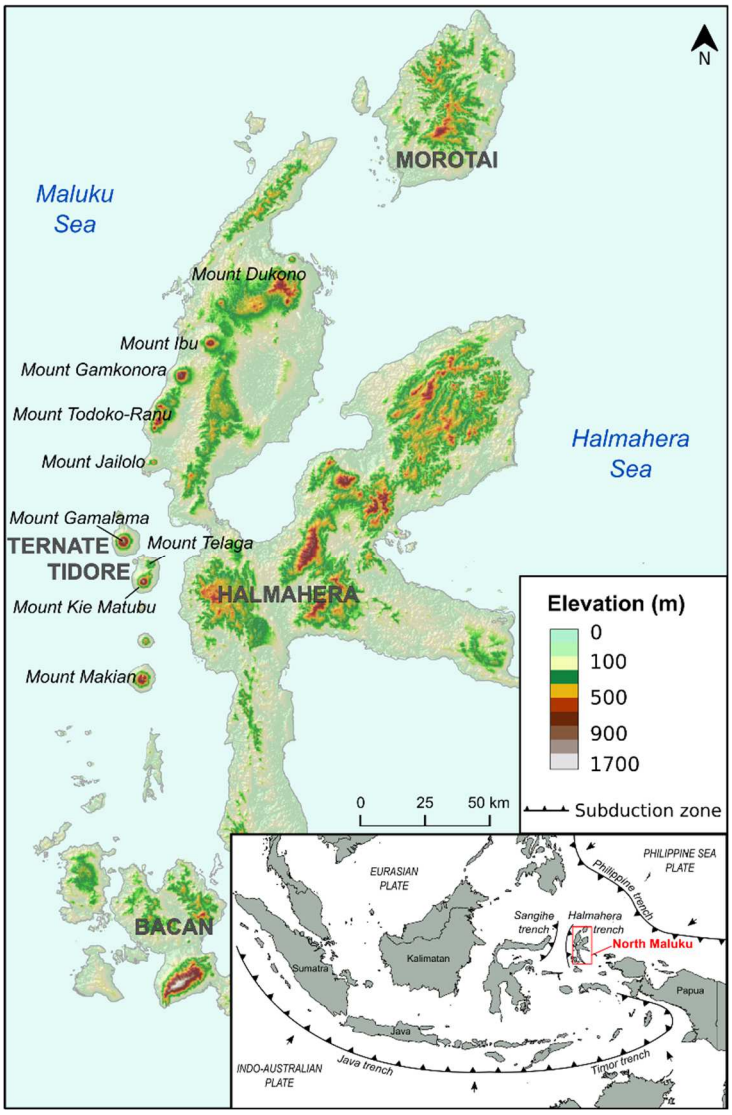

Figure 1. Map of North Maluku Province showing the study sites of Ternate and Tidore. The map is based on a ASTER DEM 30 m (acquired in October 2011) and using Arcgis 10.8.

Figure 2. Photographs of **a.** Maar Tolire northwest of Ternate, formed by a phreatomagmatic eruption in 1775. **b.** Tidore island from the Maar Ngade (view from the south of Ternate).

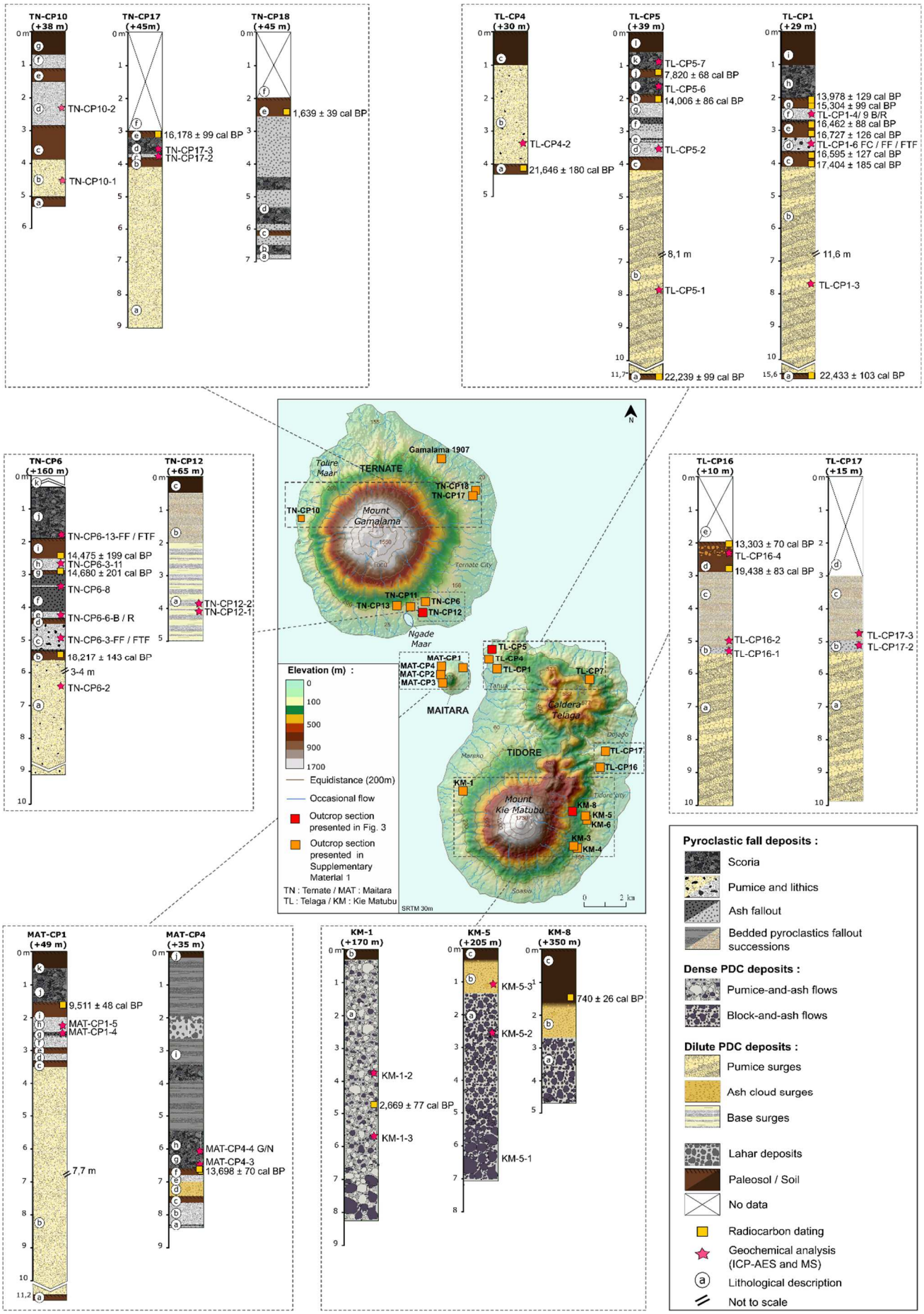

Figure 3. Location of 15 stratigraphic logs on the islands of Ternate, Maitara, and Tidore. All elevations are given in meters above sea level.

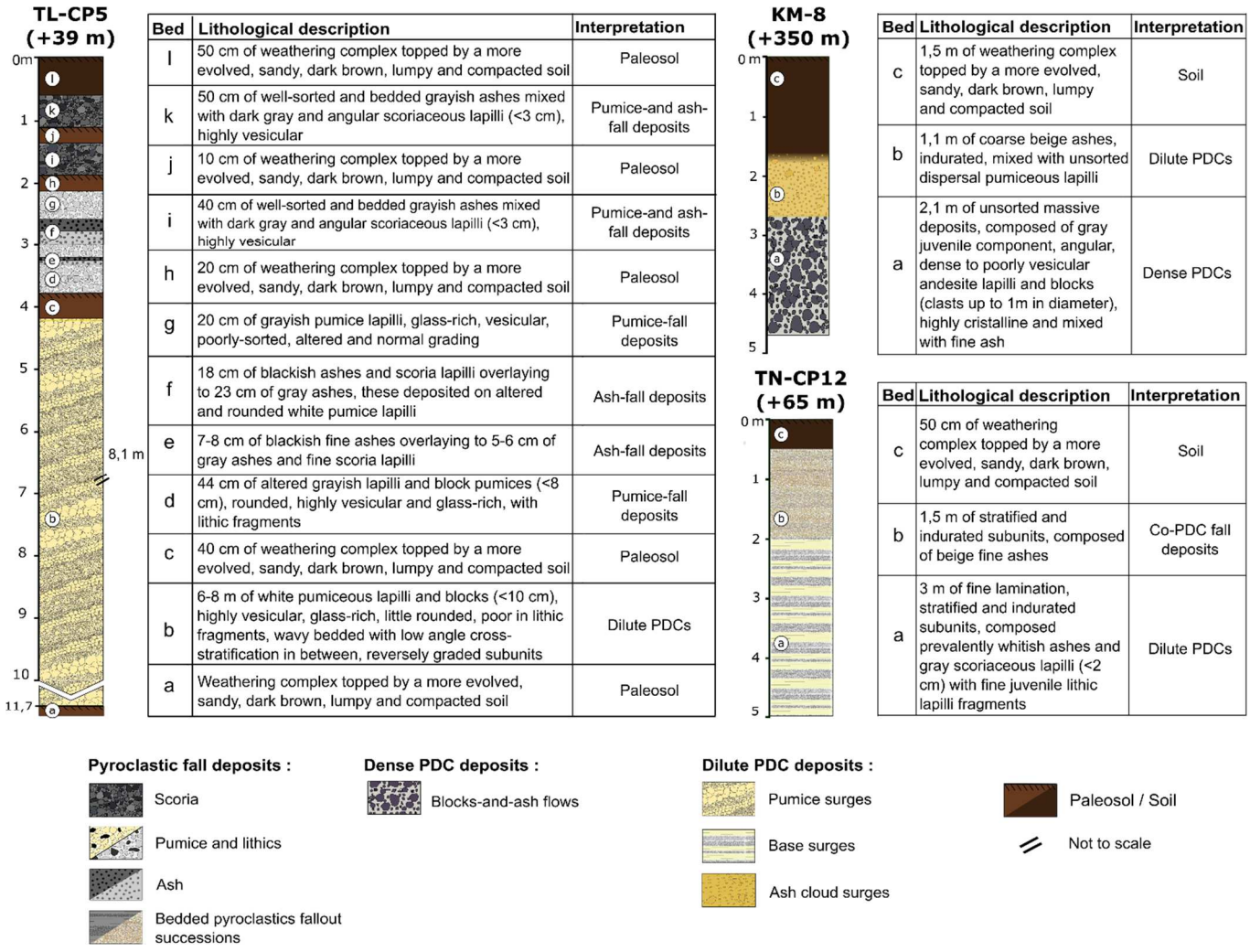

Bed	Lithological description	Interpretation
l	50 cm of weathering complex topped by a more evolved, sandy, dark brown, lumpy and compacted soil	Paleosol
k	50 cm of well-sorted and bedded grayish ashes mixed with dark gray and angular scoriaceous lapilli (<3 cm), highly vesicular	Pumice-and ash-fall deposits
j	10 cm of weathering complex topped by a more evolved, sandy, dark brown, lumpy and compacted soil	Paleosol
i	40 cm of well-sorted and bedded grayish ashes mixed with dark gray and angular scoriaceous lapilli (<3 cm), highly vesicular	Pumice-and ash-fall deposits
h	20 cm of weathering complex topped by a more evolved, sandy, dark brown, lumpy and compacted soil	Paleosol
g	20 cm of grayish pumice lapilli, glass-rich, vesicular, poorly-sorted, altered and normal grading	Pumice-fall deposits
f	18 cm of blackish ashes and scoria lapilli overlaying to 23 cm of gray ashes, these deposited on altered and rounded white pumice lapilli	Ash-fall deposits
e	7-8 cm of blackish fine ashes overlaying to 5-6 cm of gray ashes and fine scoria lapilli	Ash-fall deposits
d	44 cm of altered grayish lapilli and block pumices (<8 cm), rounded, highly vesicular and glass-rich, with lithic fragments	Pumice-fall deposits
c	40 cm of weathering complex topped by a more evolved, sandy, dark brown, lumpy and compacted soil	Paleosol
b	6-8 m of white pumiceous lapilli and blocks (<10 cm), highly vesicular, glass-rich, little rounded, poor in lithic fragments, wavy bedded with low angle cross-stratification in between, reversely graded subunits	Dilute PDCs
a	Weathering complex topped by a more evolved, sandy, dark brown, lumpy and compacted soil	Paleosol

Bed	Lithological description	Interpretation
c	1,5 m of weathering complex topped by a more evolved, sandy, dark brown, lumpy and compacted soil	Soil
b	1,1 m of coarse beige ashes, indurated, mixed with unsorted dispersal pumiceous lapilli	Dilute PDCs
a	2,1 m of unsorted massive deposits, composed of gray juvenile component, angular, dense to poorly vesicular andesite lapilli and blocks (clasts up to 1m in diameter), highly cristalline and mixed with fine ash	Dense PDCs

Bed	Lithological description	Interpretation
c	50 cm of weathering complex topped by a more evolved, sandy, dark brown, lumpy and compacted soil	Soil
b	1,5 m of stratified and indurated subunits, composed of beige fine ashes	Co-PDC fall deposits
a	3 m of fine lamination, stratified and indurated subunits, composed prevalently whitish ashes and gray scoriaceous lapilli (<2 cm) with fine juvenile lithic lapilli fragments	Dilute PDCs

740 **Figure 4.** Details of 3 stratigraphic logs representative of the two types of deposits (pyroclastic fall and PDCs) found on 15 sections (see Supplementary Material 1 for the detail of other logs).

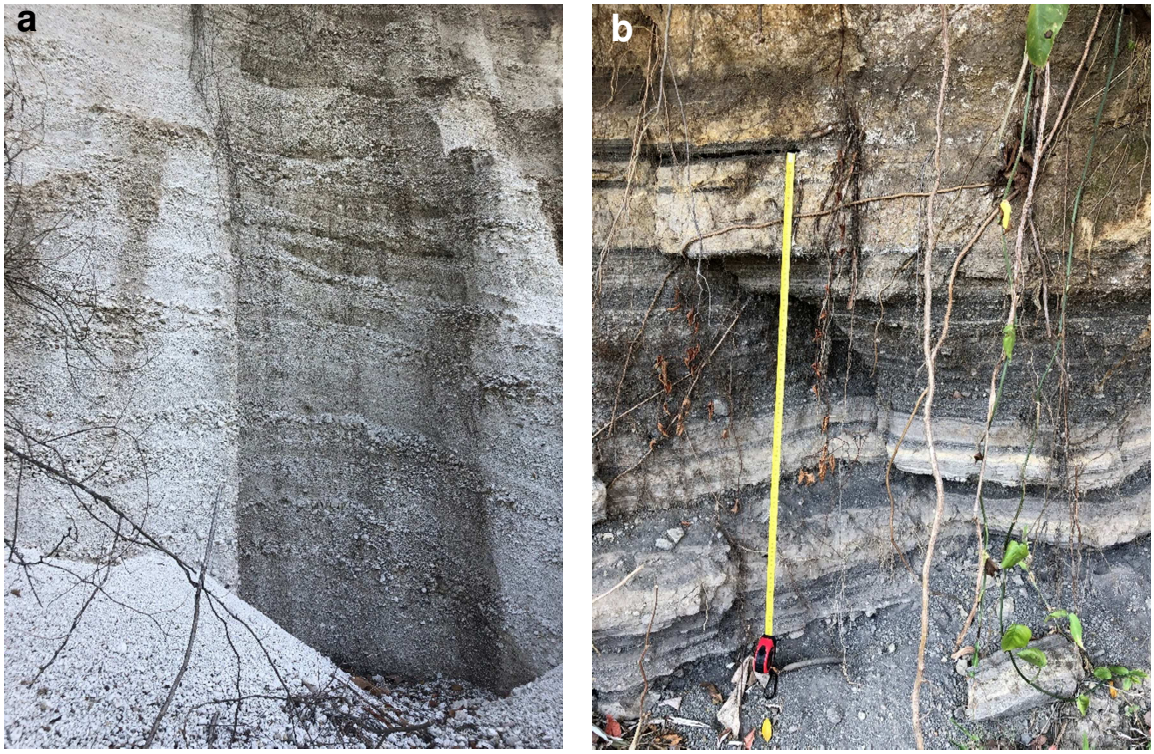

Figure 5. Photographs of **a.** White pumiceous-dilute PDCs on Tidore section (TL-CP1), wavy bedded with low angle cross-stratification in between, with reversely graded subunits. **b.** Gray ash interbedded with fine lapilli and juvenile fragments characteristic of base-surge deposits on the Ternate section (TN-CP12). The tape measure is 1 meter long.

Table 1. Summary of the PDCs features observed in all the Figure 3 sections.

PDC type	Lithological description	Sections in Figure 3
Dense PDCs (pumice- and ash-flows)	Unsorted and normal grading deposits composed of gray pumiceous lapilli and blocks (contained clasts up to 15 cm in diameter), angular, moderately vesicular and glass-rich, mixed with juvenile dense angular lapilli and blocks (>60 cm), poorly-vesicular, highly crystalline blocks	KM-1
Dense PDCs (block-and ash-flows)	Unsorted and normal grading deposits composed of gray dense juvenile lapilli and blocks (contained clast up to 1 m in diameter), angular, non-vesicular andesite component, highly crystalline, mixed white fine ash	KM-5, KM-8
Dilute PDCs (pumice surges)	White pumiceous lapilli breccia with highly vesicular, glass-rich blocks (<10 cm), little rounded, poor in lithic fragments (less than 10%). Wavy bedded deposits with low angle cross-stratification in between, reversely graded subunits	TL-CP1, TL-CP4, TL-CP5, TL-CP16, TL-CP17, MAT-CP1, TN-CP6, TN-CP10,TN-CP17
Dilute PDCs (ash cloud surges)	Indurated matrix of coarse beige-yellowish ash mixed with gray dense juvenile non-vesicular lapilli and blocks (>20 cm)	KM-5, KM-8
Dilute PDCs (base surges)	Plane-parallel or diffuse wavy-parallel stratified unit with a repetition of indurated, thin beds of coarse, grayish ash interbedded with fine juvenile lithic lapilli fragments	TN-CP12

Table 2. Radiocarbon dates of paleosols between pyroclastic deposits and one charcoal enclosed in PDC deposits. Samples are sorted by stratigraphic section. The analysis were performed at Direct AMS (WA, USA) by accelerator mass spectrometry methods. Dates were calibrated using the IntCal20 calibration curve (Reimer et al. 2020) in OxCal 4.4 (Bronk Ramsey 2020). Ages are reported at the 95,4% probability range. In each section, samples are listed in stratigraphic order, with the youngest sample on top.

Lab Code (D-AMS)	Material	Date (BP, 1σ)	Cal. BP (2σ, 95.4%)	Cal. BP (μ ± 2σ; 95.4%)	Stratigraphic Unit
30764	Paleosol	12,101 ± 87	13,783 -14,214	13,978 ± 129	Between scoria fall and pumice, below massive scoriae fallout
32715	Paleosol	12,813 ± 51	15,128-15,518	15,304 ± 99	Between scoria fall and pumice, above TL-CP1-4/9
32714	Paleosol	13,629 ± 48	16,295-16,636	16,462 ± 88	Between pumice falls, below TL-CP1-4/9
32713	Paleosol	13,784 ± 63	16,490-16,974	16,727 ± 126	Between pumice falls, above TL-CP1-6
32712	Paleosol	13,708 ± 62	16-356-16,861	16,595 ± 127	Between dense PDC (below) and pumice fall (above), below TL-CP1-6
30765	Paleosol	14,291 ± 95	17,089-17,774	17,404 ± 185	Between dense PDC (below) and pumice fall (above), above TL-CP1-3
30766	Paleosol	18,513 ± 89	22,227-22,671	22,433 ± 103	Below thick dense PDC (TL-CP1-3)
30767	Paleosol	17,819 ± 103	21,338-22,016	21,646 ± 180	Below thick dense PDC
32717	Paleosol	6,990 ± 58	7,691-7,935	7,820 ± 68	Between scoria fall
32716	Paleosol	12,134 ± 47	13,811-13,950 (29.2%) 13,967-14,140 (66.3%)	14,006 ± 86	Between pumice fall (below) and scoria fall (above)
30768	Paleosol	18,298 ± 102	22,042-22,429	22,239 ± 99	Below thick dense PDC
32711	Paleosol	18,000 ± 69	21,481-21,570 (2.6%) 21,696-22,144 (92.9%)	21,918 ± 128	Below thick dense PDC
37802	Paleosol	11,431 ± 60	13,176-13,438	13,303 ± 70	Above succession of pyroclastic fall
37801	Paleosol	16,109 ± 56	19,242-19,576	19,438 ± 83	Above succession of pyroclastic fall
32704	Charcoal	2,553 ± 24	2,516-2,590 (23.4%) 2,615-2,636 (10.6%) 2,697-2,749 (61.5%)	2,669 ± 77	Enclosing PDC
37795	Paleosol	843 ± 21	689-784	740 ± 26	Above ash fall

32709	Paleosol	8,528 ± 63	9,422-9,628 (94,3%) 9,642-9,661 (1.1%)	9,511 ± 48	Between pumice fall (below) and scoria fall (above)
37798	Paleosol	11,855 ± 49	13,531-13,536 (0.5%) 13,595-13,798 (95.0%)	13,698 ± 70	Between pumice fall (below) and scoria fall (above)
32707	Paleosol	12,366 ± 45	14,159-14,610 (70.9%) 14,675-14,840 (24.6%)	14,475 ± 199	Between pumice fall (below) and scoria fall (above)
32706	Paleosol	12,483 ± 65	14,304-15,022	14,680 ± 201	Between scoria fall (below) and pumice fall (above)
30769	Paleosol	14,899 ± 92	17,949-18,310 (86.2%) 18,495-18608 (6.3%)	18,217 ± 143	Above thick pumice-PDC
37796	Paleosol	13,434 ± 60	15,979-16,370	16,178 ± 99	Above scoria fall
37797	Paleosol	1,744 ± 22	1,570-1,706	1,639 ± 39	Above ash fall

795

800

805

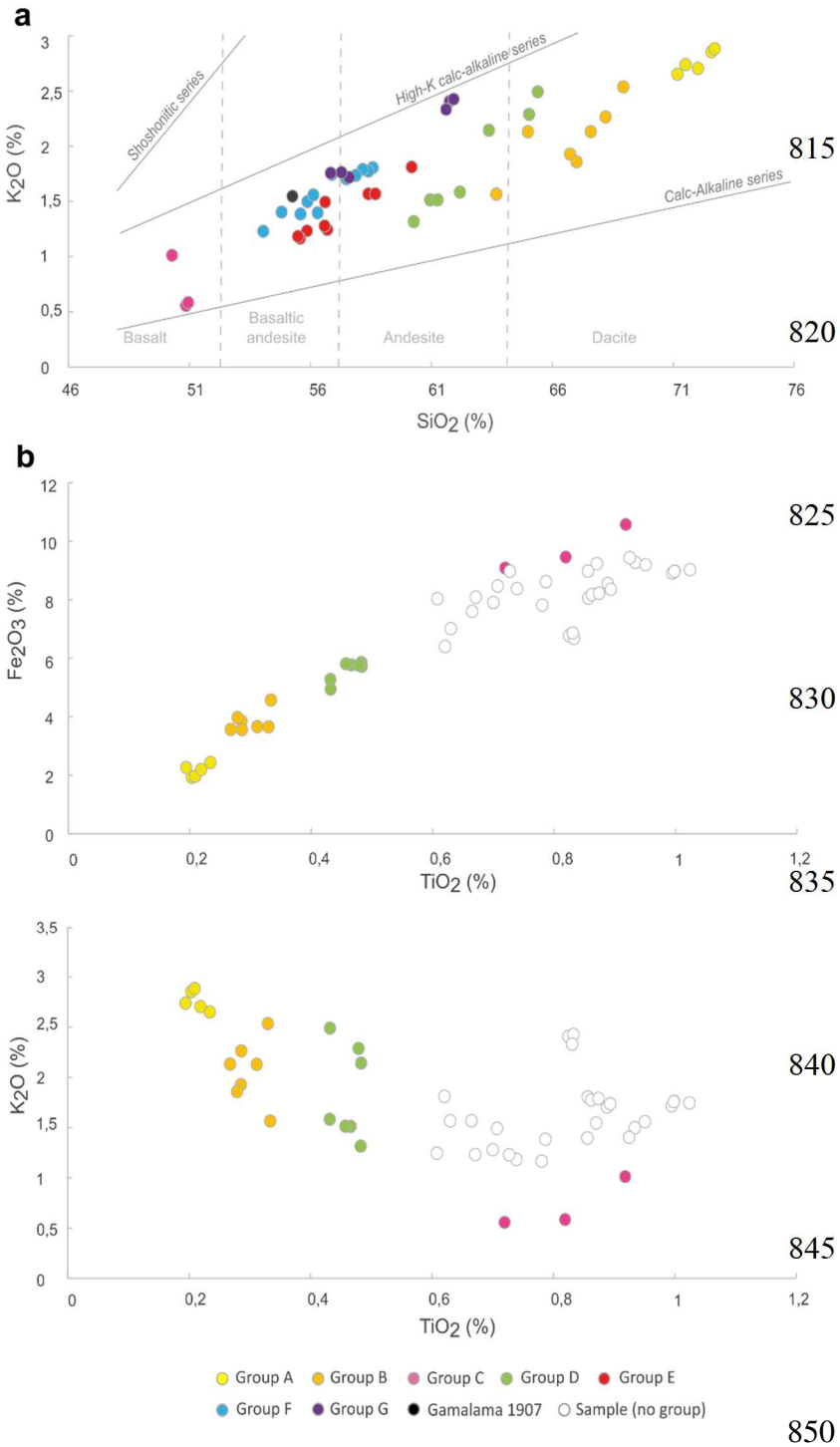

Figure 6. Diagrams with of major and minor elements on 50 samples of pyroclastic deposits from Ternate, Maitara, Tidore islands. **a.** K2O-SiO2 (%) diagram. **b.** TiO_2 (%) plotted against total iron Fe_2O_3 (%) and K_2O (%). These TAS diagrams do not include the relative uncertainties inferred from geochemical content. Major elements have been recalculated to 100% volatile-free. Analytical uncertainties between 10% (SiO_2) and 20-25% (TiO_2, Fe_2O_3, K_2O) is presented in Supplementary Material 2.

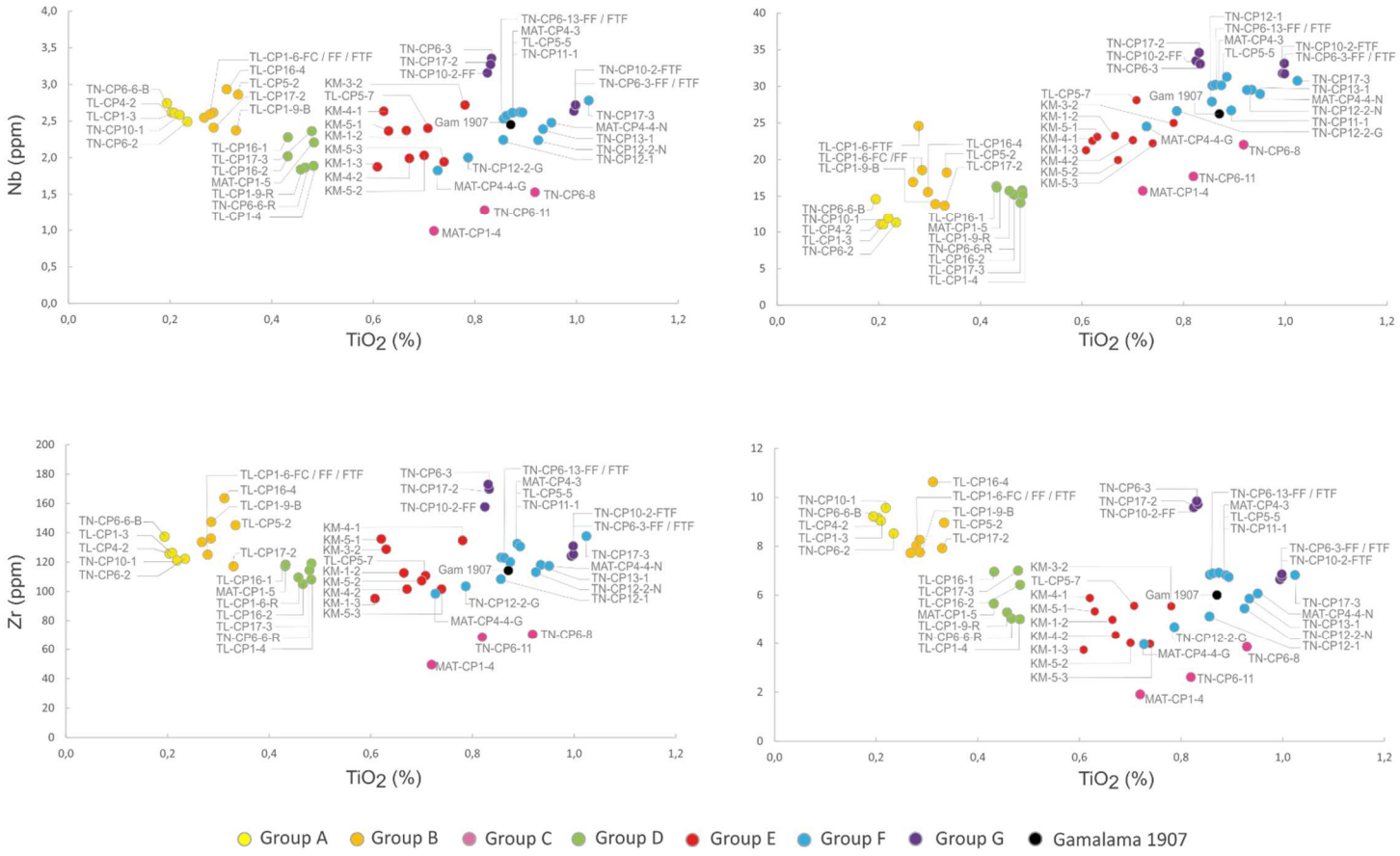

Figure 7. Binary diagrams of immobile trace elements (Th, Nb, Y, Zr) on 50 samples of pyroclastic deposits from Ternate, Maitara, Tidore islands. Major elements have been recalculated to 100% volatile-free. These diagrams do not include the analytical uncertainties inferred from the geochemical content of 6 trace elements, ranging between 5 and 15% (see further details on Supplementary Material 2).

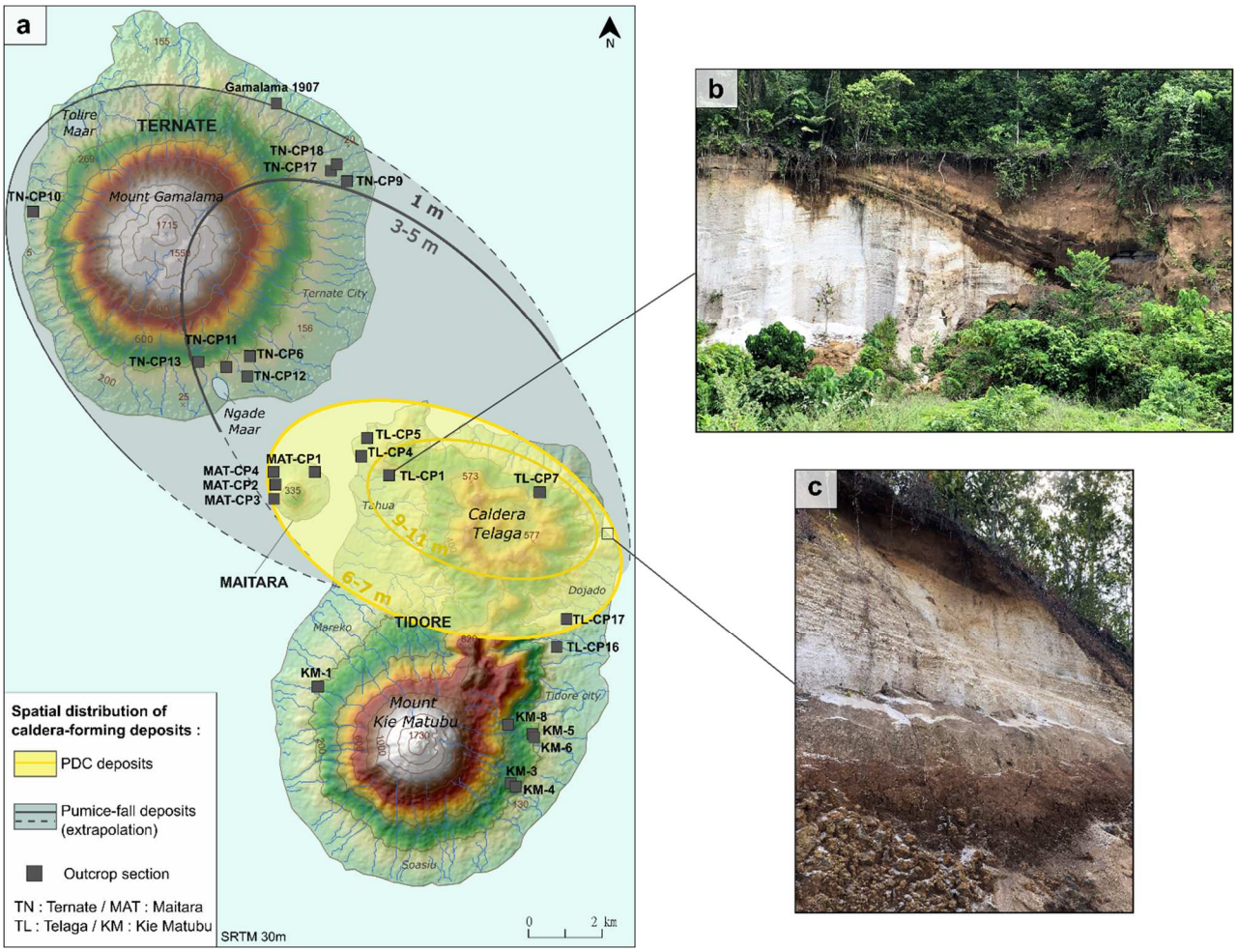

870 **Figure 8. a.** Deposits distribution of the Plinian eruption of Telaga resulting in the formation of the caldera. Photographs of massive dilute PDC deposits (pumice surges) **b.** over than 11 meters on the TL-CP1 section and **c.** at least 5 meters thick on the northeast coast of Tidore.

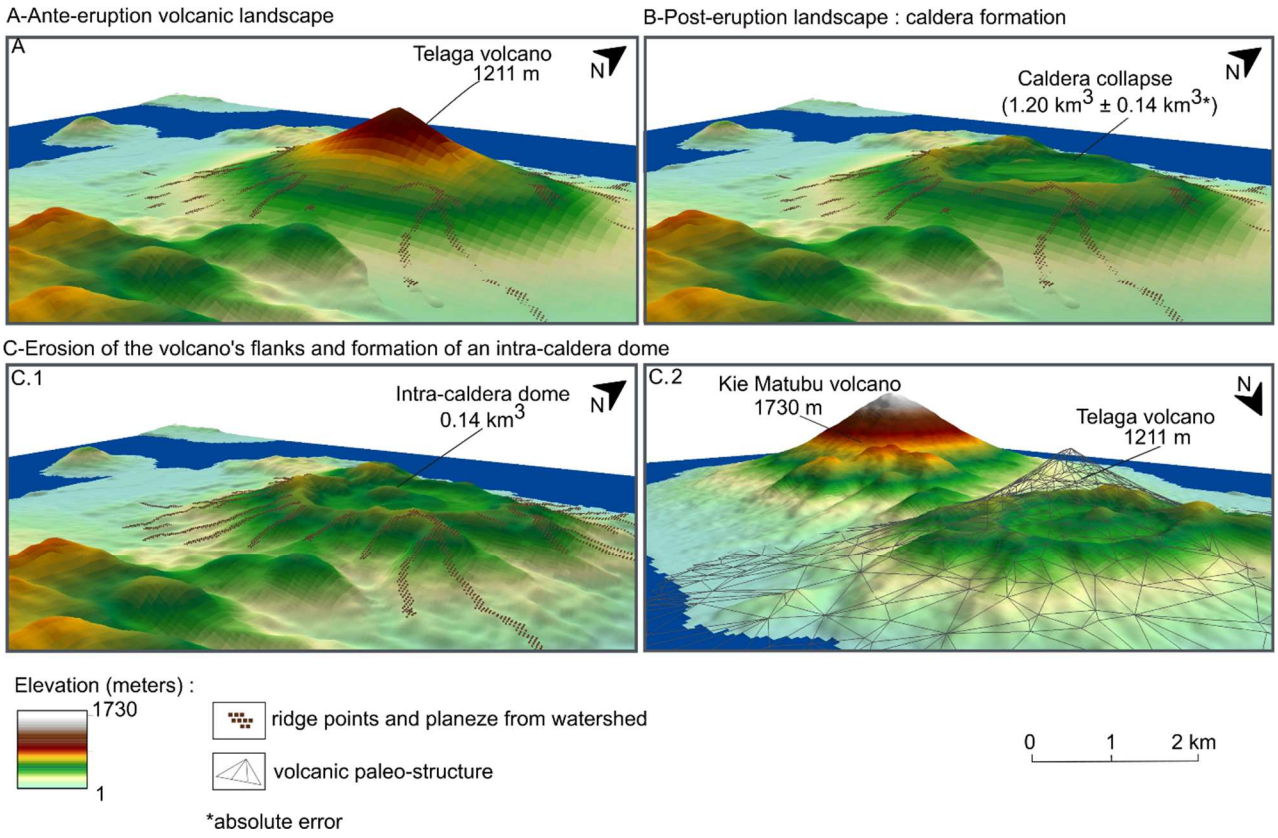

875 **Figure 9.** Topography reconstruction of Telaga volcano on Tidore island prior to the eruption with ShapeVolc software. The modeling is based on a ASTER DEM 30 m (acquired in October 2011) and using Arcgis 10.8 and ShapeVolc software developped by Lahitte. P.

880